Dripping faucet dynamics in a nonuniform electric field

Cite as: Chaos **28**, 113101 (2018); https://doi.org/10.1063/1.5040757
Submitted: 20 May 2018 . Accepted: 10 October 2018 . Published Online: 01 November 2018

T. N. Nogueira, F. A. C. Pereira, J. Procopio, and J. C. Sartorelli

Dripping faucet dynamics in a nonuniform electric field

T. N. Nogueira, F. A. C. Pereira, J. Procopio, and J. C. Sartorelli[a)]
Instituto de Física, Universidade de São Paulo, Caixa Postal 66318, 05315-970 São Paulo, Brazil

(Received 20 May 2018; accepted 10 October 2018; published online 1 November 2018)

Two experimental bifurcation diagrams were obtained with two different control parameters. One parameter was the faucet opening and the other one, keeping fixed the faucet opening, was an electrical voltage (V) applied to a metallic cylinder that surrounds the pendant water column. In this way, the drops are formed in an electrical field gradient that polarizes the water column altering the effective surface tension that is consistent with the observed decreasing of the drop mass as the potential is increased, while the water flow rate remains constant. We observed that the two bifurcations are similar for $S \lesssim 65$ and $V \lesssim 2.05$ kV; otherwise, the bifurcation evolutions are quite different. *Published by AIP Publishing.* https://doi.org/10.1063/1.5040757

The dripping faucet experiment with the flow rate as a control parameter has been suggested by Rössler to be a paradigm of a chaotic system. As a system for examining some aspects of complex systems, the dripping faucet experiment offers a collection of unique attractors and a wide range of behaviors. The novelty reported in this work is to let the drops to form in a nonuniform electrical field but with fixed water flow. We obtained similar richness of behaviors, but now with a change of a parameter that can be easily controlled.

I. INTRODUCTION

While the dripping faucet experiment presentsn itself as a paradigm of a chaotic system, its theoretical modeling is a challenging task. Many *ab initio* models were developed to describe the systems with different hypotheses and/or approaches. Schulkes[1] considered the flow as irrotational and described the system with a velocity potential. Fuchikami *et al.*[2] applied a Lagrangian description of the system. Shi *et al.*[3] and Ambravaneswaran *et al.*[4,5] constructed their model using a slender-jet approximation to the Navier-Stokes equation. The dripping faucet has also been described with spring-mass models.[6–9] These models can be seen as simplified versions of the infinite-dimensional partial differential equation models that arise from the modeling using fluid dynamics. The parameters from these models are usually estimated from the experimental data or from simulations of more complex physical models. There are also studies that analyze variations of the dripping faucet, exploring different control parameters than the water flow rate. Ilarraza-Lomel *et al.*[10] suggested in a numerical experiment the use of the magnetic field to produce variations of a magneto-rheological fluid to control the viscosity of this fluid. Reyes *et al.*[11] studied experimentally the topological aspect of the heteroclinic scenario using the nozzle inclination as a control parameter, and D'Innocenzo *et al.*[12] studied the water column oscillations as well as the dripping dynamics by breaking the cylindrical geometry of the nozzle. The effect of an electrostatic field on the shape of hanging drops was studied by Harris and Basaran,[13] and the effects of a vertical electrical field on the dripping dynamics were studied by Notz and Basaran.[5]

We are presenting the dynamics of the dripping faucet having the water flux as a control parameter as a reference for comparison against results obtained from the dripping faucet experiment in a nonuniform electrical field. Since the electrical field acts only in pendant drop, we are also showing that the applied voltage can be used as an efficient control parameter with mean water flow constant.

II. EXPERIMENTAL APPARATUS

Parts of the experimental apparatus diagram are shown in Fig. 1 (for more details, see also Refs. 14 and 15). The system operates with 1200 l of filtered and deionized water at room temperature.

It consists of a large upper reservoir (not shown in Fig. 1) that feeds an intermediary large reservoir shown in Fig. 1, in which the tap is attached, whose level is finely controlled. The tap has a linear opening gas valve driven by a step motor of 400 steps per revolution, with a reduction system that allowed us to vary the water flux by $\Delta\Phi = 1.3$ g/s/step. Therefore, we can write $\Phi = \Delta\Phi S + \Phi_0$, where S is the number of motor steps. The drops are collected in a lower reservoir (not shown in Fig. 1) and are periodically pumped back to the upper reservoir closing, in this manner, the water circuit. To measure the time between successive drops, we used a photo-diode in series with a resistor, fed by 5 V. With a horizontal laser beam focused in the photo-diode, we can detect when a falling drop starts/ends crossing the laser beam by detecting the starts/ends of the inducted pulses over the resistor. The time delays T_n between successive drops were measured with a time counter circuitry inserted in a computer slot with a time resolution of 1 μs. The dripping rate is defined as the inverse of the mean drop delays $f = 1/\langle T\rangle$, where $\langle T\rangle = \frac{\sum_1^N T_n}{N}$ and N is the total number of drops for every time series obtained. The glass faucet pipe ends in a grounded metallic nozzle placed inside a metallic cylinder tube at a potential V, as illustrated in Fig. 1, whose equipotentials were estimated by the relaxation method (see Ref. 5 for a more precise technique). To apply the voltage

a)Electronic mail: sartorelli@if.usp.br

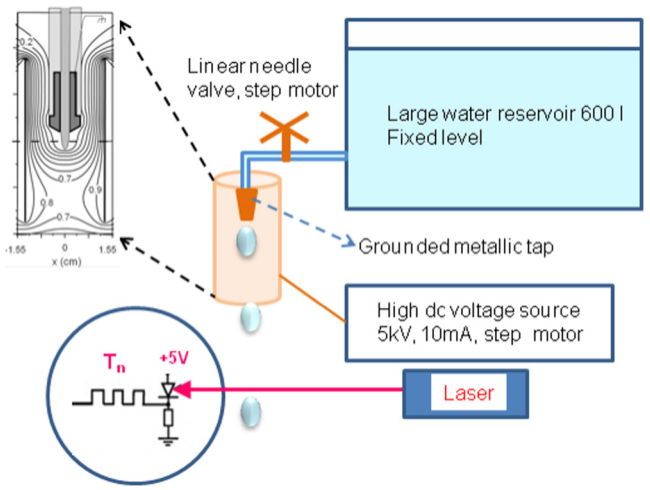

FIG. 1. Experimental apparatus diagram. Also showing details of the nozzle, $D_0 = 4$ mm diameter, inside a metallic cylinder of 2.54 cm diameter, while the metallic nozzle is grounded. The equipotentials were calculated by the relaxation method. The x axis was zoomed in twice for better visualization of the equipotential lines.

(V) to the external cylinder, we used a dc source 5 kV/10 mA whose output can be varied in multiples of 25 V.

III. RESULTS AND DISCUSSION

A. Details of drop formation in a nonuniform electric field

Our aim is to show that the voltage V applied to such a metallic cylinder can be in fact used as another control parameter in the dripping faucet experiment.[16] A complete description of the dynamics may be done in various ways, e.g., by a Lagrangian description of the system[2] or by assuming an irrotational flow.[1,4] As the numerical integration of this system is expensive and outside of the scope of this work, we will focus the discussion on a more simple and known version of the problem, that is, the equilibrium case. For that, first, we present the Fuchikami *et al.*[2] model to obtain the pendant drop profile, as sketched in Fig. 2, and then, we generalize for the case of a nonuniform electric field.

Considering that for the equilibrium case the pressure difference between the internal and external regions

$$\Delta p = p_{int} - p_{ext} = 2H\Gamma - \rho g z, \tag{1}$$

where g is the gravity acceleration, Γ is the surface tension, H is the mean curvature of the interface air-drop, ρ is the water density, and z is the vertical position of the interface. The pendant drop profile equations are given by

$$\begin{aligned} \frac{dr}{dI} &= \sin(\theta), \\ \frac{dz}{dI} &= -\cos(\theta), \\ \frac{d\theta}{dI} &= \frac{\cos(\theta)}{r} - z\frac{\rho g}{\Gamma}. \end{aligned} \tag{2}$$

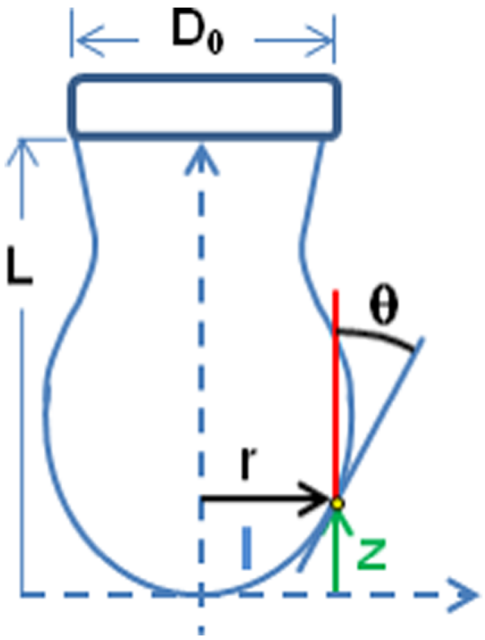

FIG. 2. Sketch of the hanging water column and the variables r, z, I, θ to be used to obtain its profile integrating numerically Eq. (2).

Therefore, the volume V_g of the pendant drop is obtained by solving Eq. (2) and integrating the following equation:

$$V_g = \frac{m}{\rho} = \int_0^{L_{max}} \pi r(z)^2 dz \tag{3}$$

until $r = r(L_{max}) = D_0/2$, the faucet radius that is the boundary condition of the pendant drop.

When we apply an electrical potential in the cylinder around the grounded faucet, the interface water/air becomes electrified; in this way, the pressure difference between the internal and the external region of the drop attached to the faucet becomes

$$\Delta p = p_{int} - p_{ext} = 2H\Gamma - \sigma_e E - \rho g z, \tag{4}$$

where σ_e is the charge density of the pending water column and E is the absolute value of the electrical field just outside the drop.

This equation suggests that the electrical field effect is to pull the droplet out of the faucet, accelerating its detachment. Simulations of a slightly different geometric setup confirm that an increase of the electrical field decreases the detached drops volume.[4] We can insert a very simplified, but dimensionally accurate, version of the curvature dependence supposing that $\sigma_e E$ can be rewritten as $\sigma_e E = 2H\alpha V^2$, where α is a constant to be determined, so we can write Eq. (4) as

$$\Delta p = 2H(\Gamma - \alpha V^2) - \rho g z. \tag{5}$$

From here, we can see that the electrical potential makes the system behave as it has modified the surface tension to $\Gamma' = (\Gamma - \alpha V^2)$ that is smaller than the water surface tension, and by applying it to Eqs. (2) and (3), the correspondent pendant drop mass was obtained.

The effect of lowering the surface tension can be seen in Fig. 3, where the attached drop mass is shown as a function of the excess pressure $p_{int} - p_{ext}$, for $z = 0$ at the bottom

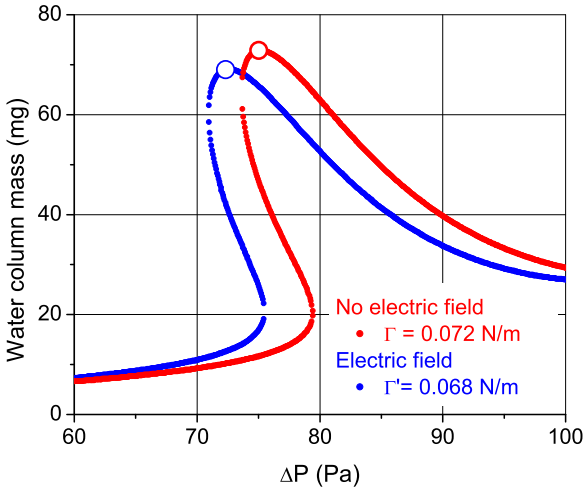

FIG. 3. Mass of the pendant drop as a function of Δp at the drop bottom for two different surface tension values. The large circles represent the critical points when the drop is detached; above these points, the pendant drop is no longer stable.

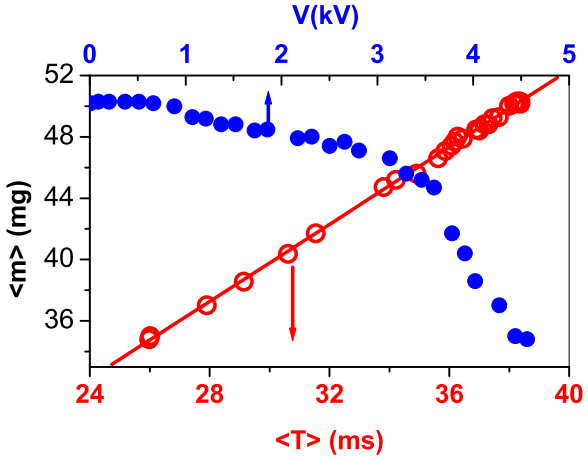

FIG. 4. $\langle m\rangle$ vs. V (top scale—blue) and $\langle m\rangle$ vs. $\langle T\rangle$ (bottom scale—red). The continuous line is the fitting to the experimental data showing that the mean water flux $\frac{\Delta\langle m\rangle}{\Delta\langle T\rangle}$ is constant.

of the drop, by solving Eqs. (2) and after integrating using Eq. (3). When there are more than one equilibrium pressure for a hanging drop volume, the stable shape is the one with smaller Δp (large circles in Fig. 3).[2] It can be seen that the reduced surface tension (blue circles) curve has a smaller maximum mass than the usual value for water (red dots). So, the expected effect of inserting the electric potential is the reduction of the drops' volumes (and masses), as the maximum stable volume gets smaller.

For each of 30 values of the applied voltage (V) in the range [0 4.5] kV, and after waiting adequate transient times, we obtained the time delays series T_n of successive drops until a volume V_{ol} was filled with N_{drops}. The mean drop mass was obtained by $\langle m\rangle = \rho V_{ol}/N_{drops}$, and the mean time of the delays between successive drops is given by $\langle T\rangle$.

The experimental mean mass $\langle m\rangle$ vs. V (top axis-filled circles) is shown in Fig. 4, as we can see that the mass drop (or size) decreases by increasing the dc voltage. We also plotted, in the same frame, $\langle m\rangle$ vs. $\langle T\rangle$ (bottom axis-empty circles). However, the mean mass $\langle m\rangle$ increases linearly with $\langle T\rangle$ in order to keep constant the mean water flux $\langle\Phi\rangle = \langle\frac{dm}{dt}\rangle =$ 1.258 g/s as shown by the straight line $\langle m\rangle$ vs. $\langle T\rangle$ fitted to the experimental data also drawn in Fig. 4.

B. Similar bifurcation diagrams $S \leq 65$ and $V \leq 2.05$ kV

First, for $V = 0$, we measured the time T_n between successive drops, having as a control parameter the faucet opening to construct a bifurcation diagram, T_n vs. S, shown in Fig. 5(a). As a second control parameter, we used the applied voltage V to the external cylinder while the nozzle is kept grounded, so we constructed the bifurcation diagram T_n vs. V, in steps of 25 V, shown in Fig. 5(b). Therefore, the pendant water column grows in a non-uniform electric field.

We have set up the dripping rate ranging from $f = 25.9$ drops/s corresponding to the $S1$ position up to $f \approx 44$ drops/s close to the maximum value of f when the hanging water column becomes continuous at the laser level. In Fig. 5(a), the letters close to the bottom x-axis refer to the following: F = fixed point, 2 = period-2, 4 = period-4, B = two chaotic bands, C = chaotic behavior, and K = also chaotic behavior. IC1 and IC2 are interior crises chaotic to chaotic, and C1 and C2 are interior/boundary periodic to chaotic crises. C3 corresponds to an interior crisis from chaotic to period-1 and to a boundary crisis from chaos to limit cycle. Examples of the chaotic profiles C can be seen in Fig. 6 and examples of K types in Figs. 7 and 8.

Keeping fixed the faucet opening corresponding to the $S1$ position [shown in Fig. 5(a)], we applied the electric voltage to the external cylinder and we obtained the diagram T_n vs. V [shown in Fig. 5(b)], and similar behaviors such as period doubling, crises, and chaotic behavior can be observed as before. Therefore, this second bifurcation diagram shows that the electric potential can be used as an efficient control parameter in a route to chaos.

For the relative faucet opening from $S = 0$ up to $S = 65$ steps (IC2 crisis), and for the applied voltage from 0 up to 2.05 kV (IC2 crisis), both bifurcation diagrams present similar

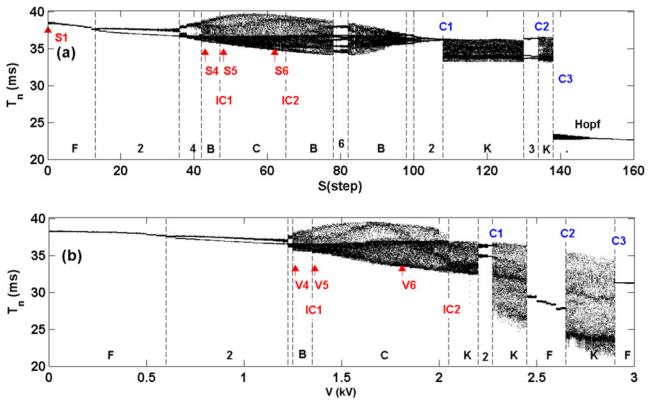

FIG. 5. Experimental bifurcation diagrams. In (a), T_n vs. S, S = the number of steps for tap opening. In (b), by keeping fixed the faucet opening corresponding to the $S1$ position, we applied the voltage V in the external cylinder, and we obtained the bifurcation diagram, T_n vs. V, having V as the control parameter, but above 3 kV some electrical sparking has occurred and the data to construct the bifurcation diagram become unstable.

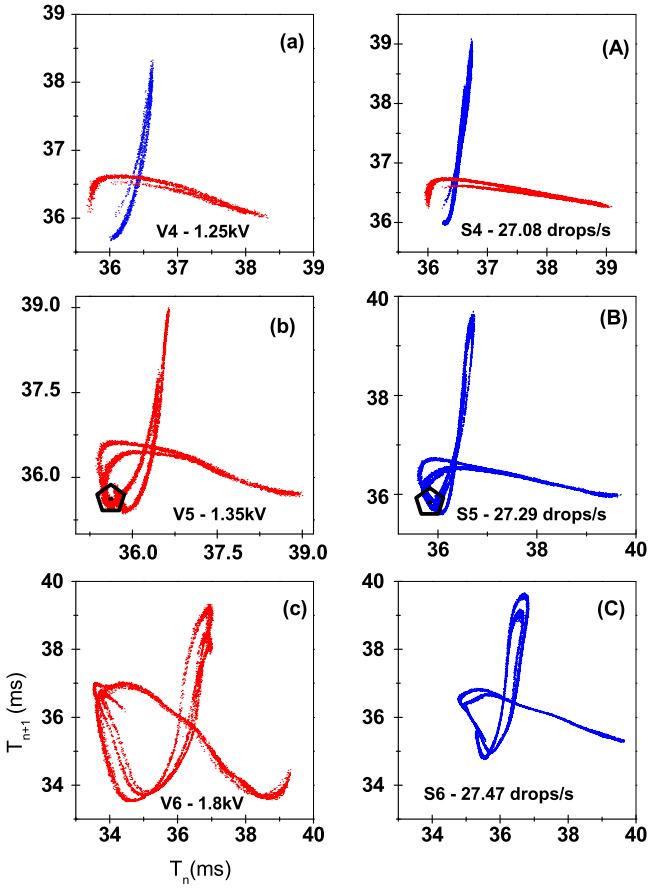

FIG. 6. On the left, attractors having the voltage as a control parameter, showing that they are similar to the ones on the right, having the faucet opening as a control parameter. In (a) and (A) examples of two chaotic bands, and below, examples of chaotic attractors type C. The centers of the black pentagons correspond to unstable fixed points.

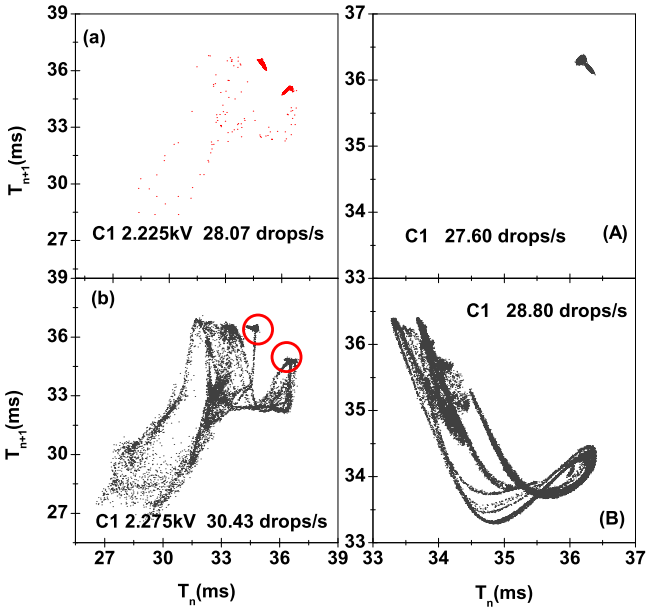

FIG. 7. Crisis C1. On the left column, we have an interior crisis from period-2 to chaos type K. Note that the period-2 attractor is embedded in the chaotic one [see red cycles in (b)]. On the right column, a boundary crisis also from period-2 to chaos type K, but the period-2 attractor is not embedded in the chaotic one.

behaviors, that is, they start in period-1 $\Longrightarrow$ period doubling $\Longrightarrow$ two chaotic bands $\Longrightarrow$ $IC1$ $\Longrightarrow$chaotic type-C $\Longrightarrow$ $IC2$ $\Longrightarrow$ for the opening case finishing in two chaotic bands but for the applied voltage in a different chaotic attractor type-K; thereafter, they follow different paths. To compare details of the two bifurcation diagrams, we reconstructed some attractors with first return maps for some values of the control parameters roughly indicated by the arrows and the labels in Fig. 5. Therefore, we are calling chaotic attractors type K the ones with different profiles of chaotic attractors type C as shown in Fig. 6.

For $V > 1\,\text{kV}$ and $S \gtrsim 42$, the similarities are less obvious. For comparison, we reconstructed the attractors for $V4 = 1.250\,\text{kV}$, $V5 = 1.350\,\text{kV}$, and $V6 = 1.800\,\text{kV}$ as shown on the left of Fig. 6 and they are to be compared with the reconstructions for the relative faucet openings $S4$, $S5$, and $S6$, respectively, also shown on the right of Fig. 6. From $V = 0$ up to $\approx 1.6\,\text{kV}$, the mean mass of the drops (so their sizes) decreases slowly (see Fig. 2), and the system follows a similar dynamics to the one having the faucet opening as a control parameter up to the $\sim S5$ position. The attractors have similar topologies and sizes, see Fig. 6, but around $V = 1.8\,\text{kV}$, and the attractors size $V6$ is bigger than the $S6$ one (see Fig. 6).

C. Crises C1, C2, and C3

Above 2.05 kV and above ∼65 steps, the two routes do not have any similarities (see Fig. 5), i.e., they present different periodic windows, crises, etc.

As an illustration, in Fig. 7 is shown the crisis labeled as $C1$ in Fig. 5. By increasing V by 25 V, a sudden change

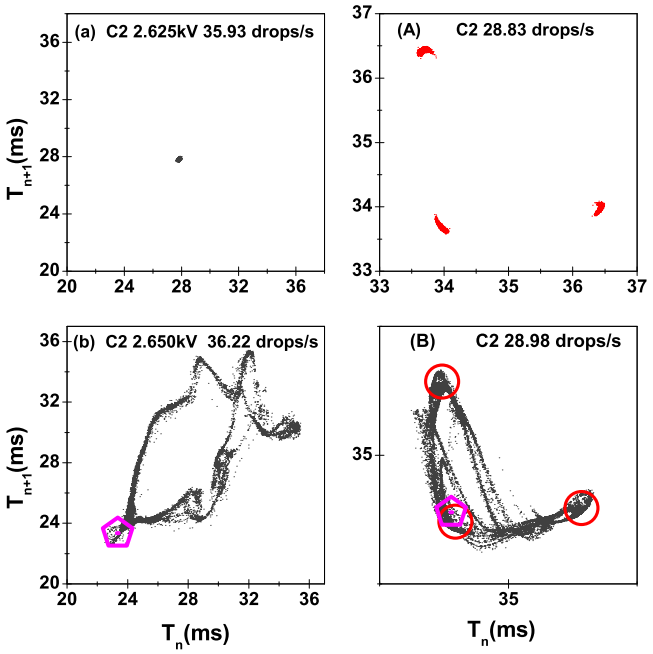

FIG. 8. Crisis $C2$. On the left, boundary crisis from period-1 to chaos type K. On the right, interior crisis from period-3 to chaos type K. In (b) and (B), the centers of the magenta pentagons correspond to unstable fixed points. In (B), the red cycles are related to the regions of visitation of period-3.

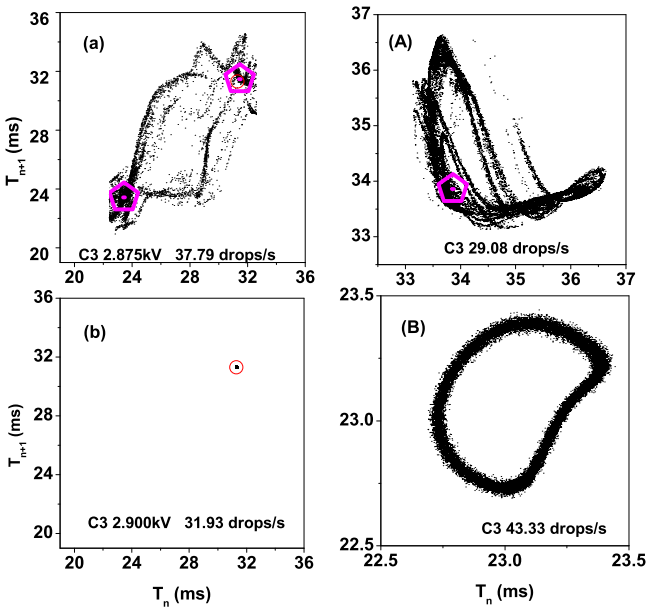

FIG. 9. Crisis *C*3. On the left, interior crisis from chaos to period-1. In (b), the red cycle corresponds to the period-1 region that is also visited in (a). On the right, a boundary crisis from chaos to limit cycle. The centers of the magenta pentagons, in (a) and (A), correspond to unstable fixed points.

occurs from a period-2 attractor [Fig. 7(a)] to a chaotic attractor [Fig. 7(b)], but this chaotic attractor evolution continues to visit the previous period-2 attractor regions, which means that its basin of attraction was not destroyed and that is a characteristic of interior crisis. Other crisis *C*1, from period-2 to chaotic attractors, occurs when we increase the opening faucet from $S = 108 \rightarrow 109$. In this case, the evolution of the chaotic attractor does not visit the period-2 regions, characterizing boundary crisis since the basin of attraction of period-2 was destroyed and replaced by the chaotic basin attractor.

The crisis labeled as *C*2 is shown in Fig. 8. On the left, we have a boundary crisis with the applied voltage, and on the right, an interior crisis, from period-3 to chaos, with the faucet opening.

On the left of Fig. 9, an interior crisis is shown, in which the system goes from chaotic to a fixed point at V= 2.9 kV. We stopped the experiment at V= 3.0 kV because the system becomes unstable due to electric sparking. On the right of Fig. 9, a boundary crisis from a chaotic attractor to a limit cycle is shown, which soon evolves to a period-1 attractor by a Hopf bifurcation until the water flux becomes continuous at the laser level and the dripping is no longer detected.

Guckenheimer and Holmes[17] describe a Hopf bifurcation by a two-dimensional map $(r, \theta) \rightarrow (r', \theta')$

$$r' = [1 + d(\mu - \mu_0)]r + ar^3, \quad \theta' = \theta + c + br^2, \qquad (6)$$

where μ is a control parameter, μ_0 is a critical control, and a, b, c, and d are constants. Thus, as long as $\mu \leq \mu_0$, the maps display quasiperiodic limit cycles of radius r_0 and rotation number ω.

As already observed by Pinto *et al.*,[14] an inverse secondary Hopf bifurcation with a glass nozzle of the same internal diameter but not so sharp as the present metallic one, we also observed such bifurcation in the same region of the

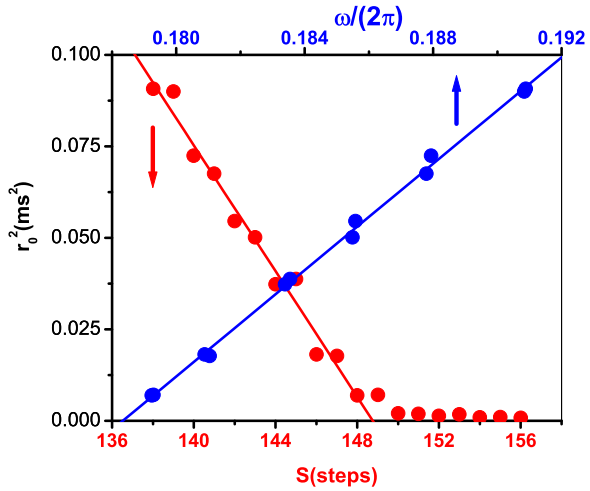

FIG. 10. Symbols correspond to the experimental data r_0^2 vs. S (bottom scale-red), a continuous line is the linear fitting of Eq. (7). Plotted in the same frame r_0^2 vs. ω (top scale—blue), a continuous line is the curve fitting of Eq. (8).

dripping rate, that is, above 40 drops/s

$$r_0^2 = \frac{d}{a}(\mu_0 - \mu) = A(S_0 - S). \qquad (7)$$

We choose $r_0 = (T_{max} - T_{min})/2$, where T_{max} and T_{min} are the mean values of T_n calculated in the last (first) bin of the ten-bin T_n histogram. The rotation numbers (in units of 2π) are obtained by the main peak position of the Fourier transforms of each time series T_n and are also related to squared radius r_0^2 by

$$r_0^2 = \frac{\omega - c}{b} = C(\omega - \omega_0). \qquad (8)$$

The experimental data of r_0^2 vs. S and r_0^2 vs. ω are plotted in Fig. 10. The continuous lines are the linear curve fittings of Eqs. (7) and (8) to the respective data $r_0^2(s^2) = 0.0086(S\text{-}148.7)\ s^2$, and $r_0^2(s^2) = 7.267[\omega/(2\pi) - 0.178]$.

IV. CONCLUSIONS

Below a critical value of the applied voltage as well as of a faucet opening without applying the potential, we have observed the same dynamical behavior in the water drop formation. Above these critical values, the bifurcation evolutions are quite different. We found that the average drop mass decreases as the potential is increased, despite the water flow rate being kept constant, which is consistent with decreasing of the water surface tension due to the electric potential applied to the external cylinder. Therefore, the applied voltage can be seen as an additional control parameter related to the variation of a physical parameter of the water. As the interaction of the nonuniform electric field occurs only in the hanging water column, we have short transient times that will allow us to study synchronizations with the oscillatory component added to the dc external electrical field and will also allow studies of parametric oscillations.

ACKNOWLEDGMENTS

This work was supported by the Brazilian agencies Fundacão de Amparo a Pesquisa do Estado de São Paulo (FAPESP; JCS 2011/19296-1, FACP 2014/07043-0) and

Conselho Nacìonal de Desenvolvimento Científico e Technológicio (CNPq; JCS 307947/2014-9).

[1]R. M. S. M. Schulkes, J. Fluid Mech. **218**, 83 (1994).
[2]N. Fuchikami, S. Ishioka, and K. Kiyono, J. Phys. Soc. Jpn. **68**, 1185 (1999).
[3]X. D. Shi, M. P. Brener, and S. D. Nagel, Science **265**, 219 (1994).
[4]B. Ambravaneswaran, S. D. Phillips, and A. O. Basaran, Phys. Rev. Lett. **85**, 5332 (2000).
[5]P. K. Notz and O. A. Basaran, J. Colloid Interface Sci. **213**, 218 (1999).
[6]R. Shaw, *The Dripping Faucet as Model of Chaotic System* (Aerial Press, 1984).
[7]L. Renna, Phys. Lett. A **261**, 162 (1999) ; Phys. Rev. E, **64**, 046213 (2001).
[8]K. Kiyono, T. Katsuyama, T. Masunaga, and N. Fuchikami, Phys. Lett. A **320**, 47 (2003).
[9]P. Coullet, L. Mahadevan, and C. Riera, Prog. Theor. Phys. Supp. **139**, 507 (2000).
[10]A. Ilarraza-Lomel, C. M. Arizmendi, and A. L. Salas-Brito, Phys. Lett. A **259**, 115 (1999).
[11]M. B. Reyes, R. D. Pinto, A. Tufaile, and J. C. Sartorelli, Phys. Let. A **300**, 192 (2002).
[12]A. D'Innocenzo, F. Paladini, and L. Renna, Phys. Rev. E **69**, 046204 (2004).
[13]M. T. Harris and O. A. Basaran, J. Colloid Interface Sci. **161**, 389 (1993).
[14]R. D. Pinto, W. M. Gonçalves, J. C. Sartorelli, and M. J. de Oliveira, Phys. Rev. E **52**, 6896 (1995).
[15]J. C. Sartorelli, W. M. Gonçalves, and R. D. Pinto, Phys. Rev. E **49**, 3963 (1994).
[16]J. A. Fornés, J. Procopio, and J. C. Sartorelli, J. Appl. Phys. **80**, 6021 (1996).
[17]J. Guckenheimer and P. Holmes, *Nonlinear Oscillations, Dynamical Systems and Bifurcations of Vector Fields* (Springer-Verlag, New York, 1986).